

The definitive version is available at <http://onlinelibrary.wiley.com/>

---

## High-resolution seismic imaging in deep sea from a joint deep-towed/OBH reflection experiment: application to a Mass Transport Complex offshore Nigeria

S. Ker<sup>1,2,\*</sup>, B. Marsset<sup>1</sup>, S. Garziglia<sup>1</sup>, Y. Le Gonidec<sup>3</sup>, D. Gibert<sup>2</sup>, M. Voisset<sup>1</sup>, J. Adamy<sup>4</sup>

<sup>1</sup> Département Géosciences marines, IFREMER, France

<sup>2</sup> Institut de Physique du Globe de Paris (CNRS UMR 7154), 4 Place Jussieu, 75252 Paris Cedex, France

<sup>3</sup> Géosciences Rennes (CNRS UMR 6118), Université Rennes 1, Bât. 15 Campus de Beaulieu, 35042 Rennes cedex, France

<sup>4</sup> TOTAL, France

\*: Corresponding author : S. Ker, email address : [stephan.ker@ifremer.fr](mailto:stephan.ker@ifremer.fr)

---

### Abstract:

We assess the feasibility of high-resolution seismic depth imaging in deep water based on a new geophysical approach involving the joint use of a deep-towed seismic device (SYSIF) and ocean bottom hydrophones (OBHs). Source signature measurement enables signature deconvolution to be used to improve the vertical resolution and signal-to-noise ratio. The source signature was also used to precisely determine direct traveltimes that were inverted to relocate source and receiver positions. The very high accuracy of the positioning that was obtained enabled depth imaging and a stack of the OBH data to be performed. The determination of the *P*-wave velocity distribution was realized by the adaptation of an iterative focusing approach to the specific acquisition geometry. This innovative experiment combined with advanced processing succeeded in reaching lateral and vertical resolution (2.5 and 1 m) in accordance with the objectives of imaging fine scale structures and correlation with *in situ* measurements. To illustrate the technological and processing advances of the approach, we present a first application performed during the ERIG3D cruise offshore Nigeria with the seismic data acquired over NG1, a buried Mass Transport Complex (MTC) interpreted as a debris flow by conventional data. Evidence for a slide nature of a part of the MTC was provided by the high resolution of the OBH depth images. Rigid behaviour may be inferred from movement of coherent material inside the MTC and thrust structures at the base of the MTC. Furthermore, a silt layer that was disrupted during emplacement but has maintained its stratigraphic position supports a short transport distance.

**Keywords:** Controlled source seismology; Seismic tomography; Acoustic properties; Submarine landslides; Atlantic Ocean

## 1. Introduction

Geophysical and geological exploration in deep-water environments has attracted considerable research effort to assess geohazards such as landslides, shallow gas and gas hydrates (Kvalstad, 2007). Undoubtedly, the perspectives provided by 3D seismic imaging techniques have yielded significant insights into the large-scale identification of such complex geological features (Bull et al., 2009; Calvès et al., 2008; Cartwright, 2007; Davies & Clark, 2006; Heggland, 2004). However, marine geohazards require quantitative seismic characterization at smaller scales for calibration with detailed measurements of geotechnical properties and sampling of the sub-seabed (ground truthing). The objective is to achieve seismic imagery consistent with the accuracy of in situ measurements, i.e. high-resolution seismic investigation at frequencies higher than 200 Hz, with consistent spatial sampling. Performing high-resolution imaging in deep water (500 m - 6000 m) encounters technological, physical and methodological issues, particularly when dealing with shallow sediment layers in the first hundred metres below the seabed (Wood et al., 2003). High-resolution seismic imaging of shallow sediments in deep-sea environments cannot be achieved with conventional near-surface seismic systems because of theoretical and physical limitations. The first limitation is technological. The source has to be sufficiently powerful to overcome transmission loss in the greater water depth: the spherical divergence of the acoustic wave in a water depth of 1000 m implies a loss of 33 dB of the effective source level. For conventional sources with a frequency content sufficiently high for high-resolution imaging such as mini air-gun, piezoelectric transducer or sparker, the source level lies in the range 190-220 dB ref. 1 Pa at 1 m and to avoid destructive cavitation, it cannot be increased. The second limitation concerns velocity analysis, the accuracy of which increases with the range of reflection angles or offsets. It is possible to increase this range of angles

by reducing the distance between the source and the reflector as with a deep-tow system, or by increasing the acquisition streamer length, as typically achieved with a near-surface system. The third limitation is one of horizontal resolution, controlled by the radius of the first Fresnel zone on the surface insonified by the acoustic wave,  $R = \sqrt{(h\lambda)/2}$  at normal incidence where  $\lambda$  is the wavelength of the monochromatic wave and  $h$  is the reflector depth. For example, for a water depth  $h = 1000$  m,  $R \simeq 40$  m when using a 500 Hz surface seismic device. The lateral resolution can be reduced down to the mean signal wavelength  $\lambda \simeq 3$  m using multichannel seismic acquisition with migration techniques (Claerbout, 1985; Scales, 1997). Limited streamer length, however, does not usually allow the required precision in velocity determination to perform sufficiently accurate imaging for this resolution to be achieved.

To overcome these limitations in high-resolution seismic imaging in deep water, one has to use (1) seismic sources/receivers with frequency bandwidths consistent with the scale of *in situ* measurements and (2) multichannel acquisition and processing techniques to increase lateral resolution. Hybrid systems based on a conventional source at the sea surface and receivers close to the seafloor, for example, those of Bowen (1984) and Nouzé *et al.* (1997), have shown improvements in the spatial resolution but this approach is not appropriate for accurate velocity analysis. A better solution is a full deep-towed device where the entire system, both the source and the receivers, operates close to the seafloor (Fagot, 1983), simultaneously providing vertical resolution improvements and better penetration into the sediment. The first full deep-towed system, called the DTAGS for Deep Towed Acoustics and Geophysics System, was developed by the U.S. Naval Research Laboratory (Gettrust *et al.*, 1991). The first version of the DTAGS had two receiver arrays of 24 channels (respectively, 2.1 m group spacing and 21 m group spacing) and a solid-state Helmholtz resonator source that emitted signals in the frequency range [250-650 Hz] (Wood & Gettrust, 2001; Chapman *et al.*, 2002). IFREMER (French Research Institute for Exploitation of the Sea) has developed its own deep-towed seismic system, called SYSIF (Système Sismique Fond), the latest version of which has two acoustic sources operating in the frequency ranges [220-1050 Hz] and [580-2200 Hz], respectively. SYSIF is therefore able to record the signals reflected from sediment layers over two resolution scales, but, to date, does not have a multichannel capability (Ker *et al.*, 2008 and Marsset T. *et al.*, 2010).

During the ERIG3D cruise (2008) on geohazards in the eastern Niger Delta, we determined the sub-seabed P-wave velocity field, avoiding the acquisition complexity of deep-towed streamer geometry, by deploying ocean-bottom hydrophones (OBHs) on the sea floor at a depth of 800 m and towing a seismic source 150 m above them. This configuration eliminated the problem of continual changes in the relative positions of the shot and receiver caused by the receiver's motion, simplifying the problem to that of the geophysical issue of depth imaging. As part of a collaboration project bet-

ween IFREMER and the French oil company TOTAL, the survey was to assess the feasibility of this approach and its value for the characterization of a large-scale buried mass transport complex (MTC), initially identified in 3D seismic data. In Section 2 of this paper dedicated to the introduction of the ERIG3D experiments, we present the geological context based on existing data, (i.e. seismic data and *in situ* measurements) and the other geophysical systems used during the cruise. Section 3 covers the joint deep-towed/OBH experiment performed during the cruise to investigate the buried MTC. Section 4 deals with the processing sequence of the streamer and OBH data, including navigation, signal processing and velocity analysis. The acquisition geometry and the improvements in these processes permit depth imaging of the OBH data through an iterative focusing approach described in Section 5. In Section 6, the resolution provided by the different geophysical devices (hull-mounted sub-bottom profiler, AUV sub-bottom profiler, deep-towed system and OBH) is compared and the data, combined with that obtained by the joint deep-towed/OBH experiment, are used to study the buried MTC. These OBH data interpreted in conjunction with sedimentological and geotechnical data provide new insights into the Mass Transport Complex; evidence of a short transport distance and rigid behaviour may indicate a slide nature of a part of the MTC.

## 2 THE ERIG3D EXPERIMENTS

### 2.1 Geological Background

The Niger Delta is a 10-12 km thick sediment wedge that has prograded onto the African continental margin and adjacent oceanic crust since the early Tertiary (Evamy *et al.*, 1978, Haack *et al.*, 2000). Gravity sliding associated with differential loading of Early to Middle Tertiary marine shales by the prograding delta has a major impact on its structural style and evolution (Knox & Omatsola, 1989; Hooper *et al.*, 2002; Morley, 2003; McClay, 2003; Corredor *et al.*, 2005). The differential load associated with uneven deltaic sedimentation is thought to have generated overpressure in marine shales and subsequent development of multiple detachment levels linking updip extension, downdip contraction and compensating translation of the intervening overburden (Morley, 2003; McClay, 2003; Corredor *et al.*, 2005; Briggs *et al.*, 2006). Extending over  $\simeq 200 \text{ km}^2$  from the shelf edge/upper slope ( $\simeq 200$  mbsl) to the mid slope ( $\simeq 700 - 900$  mbsl) the Mass Transport Complex named NG1 lies between the extensional and translational domain of the eastern Niger Delta (Garziglia *et al.*, 2009). Extension on the upper slope is accommodated by normal growth faults affecting the proximal part of NG1. Its distal part rests on the flank of a prominent dome-shaped bathymetric high formed by a shale-cored anticline whose relatively recent activity is manifested by collapse normal faults discernible on the seabed (Figure 1). The thickness of the sediment overlying NG1 is up to 120 m on the upper slope and

decreases progressively to  $\simeq 15 - 30$  m at mid slope, in 800 m water depth, where the present study focuses.

## **2.2 Seismic and *in situ* measurements**

The overall geological setting has been intensively investigated for oil prospecting. 3D seismic surveys as well as exploration and geotechnical boreholes have been drilled providing detailed regional constraints. A 3D seismic volume was courteously provided by TOTAL for this study. This conventional 3D data set has been reprocessed by TOTAL to enhance the resolution of the upper part of the volume. The processing sequence included short-offset algorithms and pre-stack time migration with inline and crossline spacing of 6.25 m and 12.5 m respectively, and the final vertical and horizontal resolutions, 7 m and 25 m. The 3D data set provides the large scale imaging of the Mass Transport Complex used in this study to evaluate the high resolution imaging method developed in this paper.

One of the objectives of the ERIG3D project, was to focus on small-scale investigation of the Mass Transport Complex. During the cruise, on the French R/V "Pourquoi Pas ?", a suite of geophysical instruments were deployed, including :

- Two sub-bottom profilers (SBP): one, a conventional hull-mounted SBP and the other a SBP mounted on an AUV (Autonomous Underwater Vehicle). Both sub-bottom profilers operate at the same frequency range [1800-5000 Hz], giving a vertical resolution close to 20 cm. Their lateral resolution is constrained by the water depth below the instrument. Whereas the AUV was deployed at the constant altitude (above the seafloor) of 80 m, giving a lateral resolution of 5 m, the water depth of 800 m restricted the lateral resolution of the hull-mounted SBP to 15 m.
- The SYSIF deep-towed seismic device: the lower frequency ranges of these acoustic sources [220-1050 Hz and 580-2200 Hz] allowed seismic images of the sub-bottom to be acquired with a metric resolution. However, the lower frequency bandwidth of SYSIF compared to SBP, allows deeper penetration in the sub-strata.
- An original high resolution seismic approach involving both the SYSIF device [220-1050 Hz] and Ocean Bottom Hydrophones (OBHs): the aim of this experiment is to provide the multi-offset recording required for velocity analysis and depth imaging algorithms. It constitutes the central subject of this paper and is therefore described in detail in the following sections, from both a technological and scientific point of view.

*In situ* measurements collected during the ERIG3D cruise were used to groundtruth the geophysical data. In addition, this study uses lithological and bulk density logs determined from the analysis of core sections of a 60 m deep borehole courteously provided by TOTAL. Bulk densities were determi-

ned from measurements of mass and volume of randomly sampled sediments. *In situ* measurements included cone penetration tests and P-wave velocity measurements (at 500 MHz). These were carried out down to 30 m below the seabed using the PENFELD penetrometer (Sultan *et al.*, 2007) developed by IFREMER (see Figure 1 for location of the measurements). The method used to interpret sediment types from the PENFELD measurements followed the approach proposed by Ramsey (2002).

### 3 SYSIF DEEP-TOWED DEVICE AND OBH EXPERIMENTS

#### 3.1 Description of the seismic devices

The SYSIF deep-towed device, designed by IFREMER and illustrated in Figure 2, consists of a seismic source and a streamer. This heavy vehicle, weighing 2.4 tons in air, is towed by the vessel with an armoured electro-optical cable delivering 1000 VAC power, and bi-directional telemetry for the seismic payload and safety controls. The navigation is achieved through four systems: the 120 kHz altimeter measures the vertical distance to the seabed, the quartz pressure sensor calculates the depth from the sea level, the miniature attitude and heading reference system measures the stability of the vehicle whilst the 14-16 kHz ultra-shortbaseline provides the relative position of the vehicle through acoustic positioning.

The SYSIF seismic source has to withstand high hydrostatic pressure; the solution was to adapt the technology of a Janus-Helmholtz acoustic transducer, initially designed for low frequency active sonars, to the needs of seismic surveying. A Janus-Helmholtz transducer consists of a piezoelectric ceramic stack inserted between two similar head-masses (Le Gall, 1999). This structure, called a Janus driver, is mounted inside a vented rigid cylindrical housing, providing a Helmholtz cavity. The coupling of mechanical resonance and fluid resonance permits a large frequency bandwidth greater than two octaves. With this performance, the seismic source is able to emit long duration frequency modulated acoustic signals, called Chirp signals, well adapted to increasing both resolution and signal to noise ratio using specific processing algorithms. The amplitude variations of the output signal due to the Transmitted Voltage Response of the transducer are taken into account through amplitude modulation. Based on this mature technology, two seismic sources have been designed: the JH250-6000 and the JH650-6000. The source JH250-6000 operates between 220 Hz and 1050 Hz, and is 112-cm high, 72-cm diameter and weighs 450 kg. The JH650-6000 for very high resolution surveys operates between 580 Hz and 2200 Hz, is 61-cm high, 45-cm diameter and weighs 90 kg. The output level of 196 dB (ref. 1  $\mu$ Pa at 1 m) over the whole frequency range is achieved using a single 6.5 kVA D-class power amplifier.

The SYSIF streamer is a dual channel antenna made of TUBA 6000 hydrophones. These hy-

drophones are piezoelectric ceramic cylinders whose high sensitivity technology of  $-193$  dB (ref.  $1$  V/ $\mu$ Pa) withstands high hydrostatic pressure without a loss of sensitivity ( $1$  dB /  $600$  bars). The first channel of the streamer is a single hydrophone with an offset of  $10$  m from the seismic source; this trace is used in the experiment to process the recorded signal amplitude. The second channel has an offset of  $15$  m from the source and is made up of  $6$  hydrophones,  $30$  cm apart and parallel-mounted to increase the signal to noise ratio. In order to prevent saturation from the direct wave, the recording uses analog electronics including a bandpass filter of  $18$  dB/octave in the range  $100$ - $3000$  Hz and a  $26.3$  dB preamplifier. Analog to digital conversion is then achieved at  $10$  kHz through a  $26$  bit ADC.

Since the device lacks multichannel technology to achieve depth imaging, Ocean Bottom Hydrophones (OBH) were deployed on the seafloor during the ERIG3D cruise to record offset data. The OBHs are autonomous recording instruments that allow the digitization of acoustic measurements of the hydrophone. Their synchronisation is achieved through a GPS clock compensated for long time drift. The storage capacity of the OBH exceeds  $1$  Gbyte, which allows four days of acquisition using a  $24$  bit sigma-delta ADC at  $5$  kHz (Auffret *et al.*, 2004; Westbrook *et al.*, 2008).

### **3.2 Deep-towed and joint deep-towed/OBH Seismic Acquisition**

The main objectives of the joint deep-towed/OBH experiments were to investigate the Mass Transport Complex NG1 both qualitatively (morphology and subsurface structure) and quantitatively (acoustic properties and P-wave velocities in particular). To reach these scientific objectives, accurate positioning of both the deep-towed system in the water column and the OBH sensors on the seafloor is a critical issue for the frequency bandwidth. The positioning of such systems, that can be accurately controlled on land or in marine surface-towed surveys, still presents many difficulties in underwater environments (Yoerger *et al.*, 2007).

During the ERIG3D experiment, five OBHs were lowered onto a flat seafloor at a water depth of  $800$  m (Figure 1b). The deployment was controlled by an acoustically navigated coring wire about  $10$  m above the seabed using an ultra-shortbaseline, i.e. an acoustic transponder measuring the travel-time of sound between the device and the vessel. The sound velocity through the water column that is required for the time to depth conversion was measured by a Conductivity Temperature Density (CTD) probe immediately before deployment. The nominal receiver spacing was  $25$  m between the OBHs with a theoretical positioning error of  $1$  % of the water depth, i.e. roughly  $8$  m around the nominal position.

Identically to the OBHs, SYSIF was positioned by an ultra-short baseline navigation system. However the time measurements were less precise because the acquisition geometry involved oblique

angles instead of straight paths. The depth and the altitude of SYSIF were measured simultaneously by a pressure sensor and an echo sounder, with relative precision of 6 cm and 12 cm, respectively.

The shot intervals for the acquisition were calculated to avoid recording the high energy multiples related to the sea surface i.e. source ghosts and seafloor related multiples; such artefacts are impossible to remove once acquired on the SYSIF section. Multiple removal techniques based on difference in move out cannot be used here and techniques based on the multiple's shape, including predictive deconvolution, also fail due to the perturbation of the waveform after reflection on the rough sea surface. We used dynamic ray tracing and computed the multiple amplitudes and travel times up to the fourth order to adapt the shot interval to our specific acquisition geometry.

The investigation of the Mass Transport Complex NG1 was carried out using the whole suite of geophysical tools available on board the "R/V Pourquoi Pas?". The reference line was therefore surveyed at different frequencies that provided a unique data set for the study of marine geohazards. The different acquisition parameters are presented in Table 1. A geological interpretation of this data set is proposed in section 6.

## **4 STREAMER AND OBH DATA PROCESSING**

### **4.1 Processing of the SYSIF navigation from joint OBH data**

Data acquisition using a towed system introduces specific variations in the fish position that tend to increase with the length of the deployed (unfurled) cable. Initially, the acquisition system is towed at a constant altitude in order to track the bathymetry of the proposed line. Using this information the depth of the system can be controlled during actual acquisition to smoothly follow this bathymetry at a constant altitude and avoid sudden changes due to abrupt variations in the seafloor. Other variations are related to the transmission of the motion of the ship to the deep-towed system through the cable, and the hydrodynamic drag of the cable. Heading and lateral motions affect the track of the deep-towed system by introducing high frequency variations in comparison to the smooth programmed variations in immersion depth. These high frequency variations in the deep-towed navigation appear as time shifts in the seismic data measured on the fixed OBHs, as illustrated on Figure 3a for the OBH3. These undesirable variations also affect the streamer data, as reported by Rowe & Gettrust (1993) on their DTAGS system. A method was proposed by Walia & Hannay (1999) to remove this 'jitter'; the overall motion was interpreted as a vertical displacement and evaluated using the recorded sea-surface reflection time to correct the seismic data to a constant depth. Taking advantage of the fixed position of the OBHs, we propose a more meticulous approach to correct the acquisition geometry and process the



jitter artefact by considering direct SYSIF-OBH travel-times in the evaluation of lateral and vertical displacements.

Raw navigation data for the SYSIF come from an ultra-short baseline positioning system. These data rely on the direct travel-times of an 8 to 17.5 kHz signal to the towing vessel, and are unevenly spaced. The accuracy of such positioning data is given as a percentage of the vertical distance between the towed vehicle and the towing vessel (1%). Other individual sensors, i.e. the altimeter and the pressure gauge, are used for real-time monitoring of the deep-towed vehicle; they produce over sampled information (0.5 Hz). Merging the navigation data from the different individual sensors is consequently a preliminary processing step to increase the accuracy in positioning.

For a more accurate navigation of the SYSIF deep-towed vehicle, we included a relocation algorithm based on travel-time inversion of the seismic signals recorded at the OBHs. The direct arrivals of the OBH traces are time windowed by a sine taper to isolate the direct arrival waveforms and then cross-correlated with the source signature (the measurement of the far field signature of the different transducers is described in the next section). The time of maximum cross-correlation corresponds to the accurate direct arrival time used for the inversion. We assess the validity of this approach with a quantitative estimator defined by Pearson's correlation coefficient (Molyneux & Schmitt, 1999 and Taylor, 1982) expressed as:

$$r(\tau) = \frac{n \sum_{t=0}^{t=n} x_0(t) x(t + \tau) - \sum_{t=0}^{t=n} x_0(t) \sum_{t=0}^{t=n} x(t + \tau)}{\sqrt{\left[ n \sum_{t=0}^{t=n} x_0^2(t) - \left[ \sum_{t=0}^{t=n} x_0(t) \right]^2 \right] \left[ n \sum_{t=0}^{t=n} x^2(t + \tau) - \left[ \sum_{t=0}^{t=n} x(t + \tau) \right]^2 \right)}} \quad (1)$$

Where  $x_0(t)$  and  $x(t)$  are two waveforms and  $\tau$  is the time of the cross-correlation maximum.

This estimator is a positive parameter whose maximum value of 1 corresponds to a perfect match between both signals. We calculated this estimator for all the shots of our experiment and then expressed the results as a function of the incidence angle between the source and the receiver (Figure 4a). During the acquisition of the SY10-HR-PR01 seismic line (Table 1), the angle range is  $[-65^\circ, +65^\circ]$  with positive values when the source is to the east of the receiver. From this result, we observe good symmetrical behavior of the system characterized by constant correlation coefficients better than 0.9 for angles  $-40^\circ$  to  $+40^\circ$  and a strong decrease down to 0.6 for higher angles. We can associate these angle ranges to the source directivity estimated from the power spectral density of the direct waveforms recorded by OBHs (Figure 4b). For angles smaller than  $40^\circ$ , the transducer directivity is negligible, corresponding to the constant correlation coefficients. For higher angles, variations in the directivity are in accordance with a decrease in the correlation coefficient. The direct waveform was considered too different from the source signature for a correlation coefficient less than 0.7; this value also being a trade-off between an accurate estimate of the travel-time and a representative number

of shots to consider in the relocation process. The value of 0.7 corresponds to a maximum incidence angle of  $\simeq 60^\circ$  or a maximum offset of  $\simeq 250$  m.

The relocation process then consists of finding the positions of both the 300 shots and the 5 OBHs utilising the signals that satisfy the correlation coefficient criterion. The inverse problem searches for the calculated direct arrival time  $tcal$  which minimizes, in the least squares sense, the difference to the observed time  $tobs$ . To solve such a nonlinear minimization problem, we apply the Trust-Region method (Byrd *et al.*, 1988 and Steihaug, 1983).

The sound velocity in the water column and the immersion depth of both the SYSIF seismic source and the OBH hydrophones are assumed to be accurate enough and do not need to be inverted in the relocation process. Therefore, the relocation procedure focuses solely on variations in position in a lateral sense.

The residuals from the inverse problem, defined as the mean values of  $tobs - tcal$ , are reported in Table 2 for each OBH. When considering only preliminary processed navigation data, two steps are followed to reduce the mean residual value higher than 1 ms:

- in step 1, the initial shot positions are kept constant to estimate the OBH coordinates using the inverse problem,
- in step 2, the revised OBH lateral positions are then used to correct the seismic shot coordinates.

As a result (Table 2), the relocation process produces a minimization of the mean residual down to  $\simeq 350 \mu s$  (except OBH5:  $600 \mu s$ ). The final displacement of the shots and OBH coordinates is within a radius of less than 10 m and is therefore consistent with the resolution of the primary navigation.

The derived lateral displacements were then applied to the primary navigation data to evaluate the original processing from the joint deep-towed/OBH acquisition. The approach consisted of fixing a datum plane for the SYSIF source depth, computing the associated direct arrival times  $tnew$  and then evaluating the differences  $tobs - tnew$ . This time correction is given by the expression:

$$\Delta t = \frac{1}{c_w} \left[ \sqrt{(\mathbf{x}_s - \mathbf{x}_r)^2} - \sqrt{(\mathbf{x}_{s,z=z_0} - \mathbf{x}_r)^2} \right] \quad (2)$$

with  $c_w$  the sound velocity in the water column given by the CTD probe,  $\mathbf{x}_s$  and  $\mathbf{x}_r$  the source and receiver positions, respectively;  $\mathbf{x}_{s,z=z_0}$  stands for the source coordinates with a constant immersion depth of  $z_0$ . The results of applying this relocation correction on the OBH traces are shown in Figure 3. The improved lateral coherency of the reflected waves clearly demonstrates the validity of the relocation procedure.

## 4.2 Chirp signal processing from real source signature

The conventional signal processing method used in marine sub-bottom profiling (Quinn *et al.*, 1998) is to cross-correlate the recorded traces with a theoretical pilot signal or with the direct wave recorded at the nearest hydrophone (Chapman *et al.*, 2002, He *et al.*, 2009). The effect is to compress the signal at the reflected horizons.

The limit of this approach is based on the assumption that the pilot signal matches the real output source signal, i.e. the transfer function of the seismic source including the power amplifier, the impedance matching unit, the transducer, etc., can be considered to be negligible, which is obviously not true. A more meticulous signal processing consists of considering the *in situ* far field measurement of the source to perform signature deconvolution (Ziolkowski, 1991); this solution is not straightforward and requires specific source signature measurements at sea.

In order to evaluate this approach, we designed and performed sea trials in May 2009 to record the far field seismic signatures of both the JH250-6000 and JH650-6000 transducers. A dedicated signature hydrophone (HighTech HTI90 hydrophone), connected to an autonomous analog recorder, was anchored at a distance of 12 m below the SYSIF deep-towed vehicle (the value of 12 m is consistent with far field signature constraints as our lower frequency is 220 Hz, i.e. 6.7 m wavelength). In order to avoid interference from echoes from either the sea bottom or the sea surface, the measurements took place in 2000 m of water with the SYSIF being lowered to 1000 m below the stationary vessel.

The measurements underlined the excellent repeatability of both sources. The differences between the far field signature and the pilot signal are clear and reflect not only the transfer function of the sources but also a strong resonance frequency associated with the Helmholtz cavity at 300 Hz (Figure 5). This confirms that a source signature deconvolution approach is preferable to conventional correlation processing which would have blurred the structures in the final seismic processing (Brittle *et al.*, 2001).

The deconvolution procedure is based on the convolutional model which states the seismic trace is the convolution between the source signature  $s(t)$  and the geological reflectivity  $r(t)$ . In the presence of noise  $n(t)$ , the seismic trace is expressed as:

$$x(t) = s(t) * r(t) + n(t) \quad (3)$$

A source signature deconvolution is then defined by a division in the Fourier domain (Yilmaz, 1987):

$$\frac{X(\omega)}{S(\omega)} = \frac{R(\omega)S(\omega)}{S(\omega)} + \frac{N(\omega)}{S(\omega)} \quad (4)$$

Where  $\frac{X(\omega)}{S(\omega)}$  is the deconvolved trace in the Fourier domain with  $X(\omega)$ ,  $S(\omega)$ ,  $R(\omega)$ ,  $N(\omega)$  are the Fourier Transform of, respectively, the data, the source signature, the geological reflectivity, and

the additive noise. In practice, a noise factor has to be added to the source before the division so as to prevent any division by zero and to reduce the amplification of noise.

OBH data present excellent signal to noise ratio exceeding 36 dB and therefore, on this particular data set, the noise factor is not necessary to ensure the stability of the division. The streamer data is also characterized by a high signal to noise ratio (27 dB) which may be related to the performances of the receiver, to the "peaceful" deepwater environment and to the low speed of the acquisition (1-2 knots). As a qualitative result, a comparison between the conventional correlation and the signature deconvolution is shown in Figure 6: the differences in the lower part of the section where the signal to noise ratio is minimum are clear. A 350-1100 Hz band-pass frequency filter has been applied in the correlation section (Figure 6a) to avoid the Helmholtz resonance frequency whereas the filter bandwidth was 200-1100 Hz in the deconvolution section (Figure 6b) to attenuate frequencies outside the emitted bandwidth.

As a quantitative result, we can estimate a vertical resolution of the imaging process between 0.5 and 1 m, thanks to both the large frequency bandwidth of the source and the successful signature deconvolution. Moreover, the low altitude of the deep-towed vehicle above the seafloor (150 m) allows a good lateral resolution, between 15 m and 20 m depending on the reflector depth to be achieved.

### 4.3 Analysis of the sub-surface velocity profile in the time domain

Unlike surface seismic records, the locus of reflection points for each source-receiver pair in our OBH survey changes with reflector depth. In a horizontally layered medium, this locus tends towards the source-receiver midpoint with increasing depth. Therefore, the OBH data cannot be sorted into CMP gathers and the NMO velocity analysis has to be carried out on receiver gathers. The geometry of the acquisition is asymmetrical due to the difference in altitude between the source and the receiver; thus, we have to redefine the travel time equation of reflected events and to adapt the NMO approach to this particular case. For the sake of simplicity, we consider a strictly 2D acquisition geometry (where both the receiver and the source are on the same plane). The receiver is located on the seabed and if we assume flat underlying layers, the arrival time of the P-wave reflected wave at the interface  $n$  is thus expressed as:

$$t^2 \approx t_{0,n}^2 + \frac{x^2}{\bar{V}_n^2} \quad (5)$$

Where  $t_{0,n}$  is the zero offset arrival time of the P-wave reflection at the interface  $n$ ,  $x$  is the horizontal distance between the source and the receiver (offset) and  $\bar{V}_n$  is the root mean square velocity.  $t_{0,n}$  and  $\bar{V}_n$  can be expressed in function of  $v_k$  and  $d_k$  which are respectively the P-wave interval velocity and thickness of the  $k$ -th layer. The first layer is the water column.

$$t_{0,n}^2 = \left[ \sum_{k=1}^{k=n} \frac{d_k}{v_k} + \sum_{j=2}^{j=n} \frac{d_j}{v_j} \right]^2 \quad (6)$$

and  $\bar{V}_n$  the quadratic velocity expressed as:

$$\frac{1}{\bar{V}_n^2} = \frac{\sum_{k=1}^{k=n} \frac{d_k}{v_k} + \sum_{j=2}^{j=n} \frac{d_j}{v_j}}{\sum_{k=1}^{k=n} v_k d_k + \sum_{j=2}^{j=n} v_j d_j} \quad (7)$$

This formulation of the travel time is similar to the one used in offset vertical seismic profile processing which shares its asymmetrical acquisition geometry with our OBH experiment (Dillon and Thomson, 1984).

To perform the P-wave velocity analysis, negative and positive offsets, corresponding to OBH positions on the east and west side of the SYSIF seismic source were considered separately. The semblance panels for OBH3 are shown in Figure 7. An average P-wave velocity of between 1480 and 1490 m/s would be interpreted for the sedimentary cover located in the first 200 ms below the sea bed. This value appears consistent for both positive and negative offsets. Below 200 ms, the velocity gradients differ and having opposite signs would seem to suggest that the flat layer assumption is no longer valid. The semblance analyses for the other OBH locations confirmed these results and in particular the presence of a constant velocity in the first 200 ms.

## 5 DEPTH IMAGING OF THE MASS TRANSPORT COMPLEX FROM OBH DATA

### 5.1 Velocity Analysis by a depth focusing approach

Since the velocity analysis in the time domain appears to fail in the deeper part of the section, we proposed to work in the depth domain to apply a more accurate analysis through an iterative migration process. A classical approach for velocity analysis in the depth domain consists of migrating the data separately for each offset gather and to assess the flatness of a given reflector (Al Yahya, 1989). Nevertheless, this approach had to be modified in order to take into account the particular geometry of our acquisition; the velocity analysis has been evaluated on the depth migrated receiver gathers instead of on the offset gathers. On the depth migrated receiver gathers, underestimation and overestimation of the P-wave velocities will induce a bending in the reflector shape. This "bending" criterion is only valid for reflectors with simple geometry; previous analysis of 3D seismic data in the studied area has shown that this assumption is acceptable.

The Kirchhoff migration (Schneider, 1978 and Scales, 1997) appears to be the most appropriate method as it easily handles the particular geometry of our experiments. The Kirchhoff algorithm requires the computing of travel-time tables between the SYSIF seismic source and the OBH hydro-

phones. We calculated these travel-time values by solving the Eikonal equation through a finite difference algorithm (Podvin & Lecomte, 1991).

Initially, depth migrations were performed on receiver gathers using constant RMS velocities ranging from 1460 to 1500 m/s at intervals of 10 m/s. The resulting depth images are presented in Figure 8 where the bending of the reflectors deeper than 810 m demonstrates the sensitivity of the data to RMS velocity variations finer than 10 m/s. It was decided that using interval velocities for the depth migration may give better results.

The determination of the interval velocities was then carried out using a horizon consistent layer stripping approach. In an iterative process where the interval velocity is determined layer per layer using constant velocities. The shape criterion is applied to the reflection, which delimits the bottom of a layer, to define the velocity that best fulfills the criterion. In order to perform this iterative process, we modelled the subsurface structure with four major geological horizons, including the seabed. The water velocity was derived from CTD measurement. In the shallow part of the section there are almost no contributions to the seabed reflector due to aperture limitation and the absence of continuous reflectors inside the Mass Transport Complex. The velocity of the upper sedimentary layers (up to 840 mbsl) was therefore obtained from the results of the previous constant velocity migration (1480 m/s). The iterative process then focused on the deeper part of the section.

The final depth section from OBH3 is presented in Figure 9 together with its associated interval velocity distribution and the corresponding time section recorded with the streamer (SY10-HR-Pr01). The horizons selected to perform the depth focusing approach are located respectively at 845, 900 and 920 m. *In situ* velocity measurements from Vp13S03 (data from the Penfeld Penetrometer) are also presented in Figure 9 to demonstrate the almost homogeneous behaviour of the velocity distribution in the upper part of the section.

## 5.2 Characteristics of the OBH Depth Images

In this section, further details of the depth images obtained from the OBH are provided in terms of illumination, sensitivity to the 2D approximation in the imaging procedure and velocity uncertainties.

Regarding the reflector illumination, it is worth highlighting the difference between the streamer and the OBH experiment. In the OBH configuration, the asymmetry of the acquisition leads to a different illumination compared to surface conventional imaging as already mentioned in section 4.3. Thus, in the case of flat layers, the segment  $D$  of a reflector at the depth  $d$  illuminated by the hybrid geometry is given by:

$$D = \frac{L_S}{2 + \frac{h}{d}} \quad (8)$$

Where  $L_S$  is the maximum distance between the source locations and  $h$  is the altitude of the seismic source.

This formula demonstrates that for our specific acquisition geometry, the lateral extension illuminated by the experiment is smaller than that achieved with conventional acquisition. Therefore, the shallower the reflector, the smaller the illuminated part of the reflector but the denser the illumination of this reflector segment will be. This dense illumination guarantees the success of the Kirchhoff approach (large numbers of rays contributing to building the depth image) for OBH data and explains the achievement of detailed depth images (lateral resolution close to 2.5 m) in the vicinity of OBHs.

The positioning processing phase has demonstrated that the strictly non-2D nature of the acquisition geometry of our experiment does not allow the projection of all the source and receiver locations onto a single line. Thus, each OBS has to be processed with its own line of projection and the final depth images do not belong to a unique plane. The maximum distance between depth section planes is however less than 10 m.

Regarding a single OBH, the projection onto a 2D line certainly adds errors in the velocity estimation, as the apparent velocity is smaller than the average velocity due to the underestimation of the travel path. The comparison of travel times using 2D and 3D ray tracing allows the uncertainties in velocity associated with the 2D projection to be evaluated to 10 m/s for the shallowest reflectors and negligible for the deeper ones.

Despite these theoretical limitations, we investigated the possibility of performing a stack with the five OBH images. A common projection line was first defined by linear regression to allow the binning of OBH traces. To preserve amplitudes, the edges of the gathers were trimmed to remove the migration artefacts before stacking and a weighting factor was applied that was related to the contribution of each pixel of the OBH images to the final stack depth section. A comparison of this OBH depth section with the corresponding streamer time section is presented in Figure 10. Before the interpretation of this depth section, we have to stress on the assumptions made during the stack procedure. Pitfalls in the interpretation may exist due to the summing of reflections that are not actually in the same plane. Since these pitfalls may arise essentially in the shallow part of the section, the interpretation of the top of the MTC was carried out with single OBH depth sections.

The additional contributions to the understanding of the Mass Transport Complex NG1 from the interpretation of the results of the OBH acquisition/processing sequence will be discussed in the next paragraph.

## 6 INSIGHT GAINED INTO THE CHARACTERIZATION OF THE STUDIED MASS TRANSPORT COMPLEX

### 6.1 Towards an increasing resolution of the NG1 MTC Image

The aim of the ERIG3D cruise and its associated project was to assess a more appropriate geophysical investigation approach to characterize geohazards in deep sea environments and to allow the correlation between acoustic and ground truth data. An ideal geological object where such a quantified approach could be conducted is NG1, a buried Mass Transport Complex identified in this area. It is a MTC with strong structural complexity where many different geophysical methods have been deployed, in particular the deep-towed system and the first joint deep-towed/OBH system presented in the previous sections. The progressive improvements in image resolution and the consequence to the geological comprehension of the NG1 Mass Transport Complex can now be illustrated through the seismic sections of the NG1 acquired by the different geophysical systems.

To improve the vertical resolution, NG1 was surveyed four times using two different sub-bottom profilers (hull-mounted and AUV-mounted [1800-5000 Hz]) and the two configurations of the SYSIF apparatus ([220-1050 Hz] and [580-2200 Hz]). The profilers are limited to single-fold acquisition and therefore their lateral resolution is controlled by their altitude above the seabed. This observation is illustrated with the comparison of the hull-mounted SBP (mean frequency 3000 Hz) and the high frequency SYSIF seismic source (mean frequency 1200 Hz) proposed in Figure 11. For the current water depth (800 m) and the altitude of the SYSIF (80 m), the theoretical lateral resolutions are respectively 6 m for the SYSIF and 14 m for the hull mounted SBP. The lateral resolution improvement in the SYSIF line is obvious despite its lower frequency, thus making possible the interpretation of the front of NG1 whereas the SBP image is blurred with hyperbolae.

The first seismic data set involved in the study of NG1 was a conventional exploration 3D cube re-processed with a pre-stack time migration of the short offset traces to enhance the final resolution. The line presented in Figure 12a was extracted from this 3D cube and reveals the large-scale structure of the Mass Transport Complex NG1. The vertical and lateral resolution of this profile are evaluated at 7 m ( $\lambda/4$ ) and 25 m ( $\lambda$ ), according to the mean frequency of the signal (60 Hz). Profile AUV03-Pr16 and profile SY10-HR-Pr01 were acquired at the same location as the 3D cube profile. Compared to this profile, the improvement in resolution is obvious and the small scale structures can now be clearly identified (Figures 12b and 12c). The upper sedimentary cover (20 ms) is imaged in greater detail with the AUV, nevertheless, even with its high frequency content and its limited sound level, the SBP does not provide insights either into the top, nor into the basement of NG1. The SYSIF [220-1050 Hz] deep-tow appears as the seismic system which provides the best vertical resolution (0.5-1 m) showing



details of the entire Mass Transport Complex structure, from its top to its base. Nevertheless, its lateral resolution is still limited to the Fresnel zone (15 m) as underlined by the hyperbolae at the top and at the bottom of the NG1 complex.

The results of the joint deep-towed/OBH experiment, described here, allowed previous limitations to be overcome and the lateral resolution to be enhanced down to the mean frequency wavelength, i.e. 2.5 m, over the whole OBH section (Figure 13). The main consequence in the seismic imaging of NG1 is the removal of the diffraction hyperbolae. The approach allows the high amplitude reflections marking the top of NG1 to be emphasized. At the base of NG1 high amplitude overlapping reflections outline complex deformation patterns. In Figure 13 the seismic section from OBH3 shows reflections at the top and base of NG1 that are sub-parallel with dips of  $\simeq 6^\circ$ .

## **6.2 Geological Insights on NG1 MTC and confrontation to *in situ* measurements**

The following discussion aims to highlight the geological insight provided by the joint deep-towed/OBH experiment by comparing the features genetically associated with mass transport deposits that have been identified with this new approach with those seen with a conventional approach based on 3D seismic and sub-bottom profiler data.

Based on the interpretation of the 3D seismic data and chirp data, both the internal incoherency and the diffracting top characterize a debris flow that implies mass transport over large distances and the consequent disintegration and disorganisation of the material (see Canals *et al.*, 2004). However, as discussed by Tripsanas *et al.*, 2008, debris flows may share the same seismic and sedimentary characteristics with slides that, by contrast, have been transported over relatively short distances and preserve their primary stratification.

Some evidence that may support a slide nature of a part of the NG1 MTC can be obtained from the high resolution OBH depth images and the integration of *in situ* measurements with the seismic data:

- Rigid behaviour may be inferred from movement of coherent blocks that can be interpreted from the analysis of OBH depth images showing that, locally, the basal and upper part of NG1 are tilted by the same amount (Figure 13). The finer details in these images provide unprecedented information about the imbricate thrust character of NG1 basal part, indicating restricted movement of a coherent mass.
- Transport over short distances is supported by the integration of the available data. By providing depth images with vertical/horizontal resolution of 0.5-1 m / 2.5 m, the joint deep-towed/OBH data serve as a reliable intermediary for extrapolating fine scale analysis on core and *in situ* measurements across seismic lines. The CPT09S05 profile tied to the OBH3 depth image shows a set of high ampli-

tude reflections observed on top of NG1 at site BH-FP7. These possibly represent the occurrence of a 30 cm thick layer observed in borehole core section and identified on the density log by an abrupt increase up to  $1.6 \text{ g.cm}^{-3}$  (Figure 14). If this is the case, the silt layer was disrupted during the emplacement of NG1 while maintaining its stratigraphic position.

## 7 CONCLUSION

Deep sea geohazards require to be characterized at fine scales by high resolution seismic imagery that enables correlation with ground truth data. In this paper, we described an experiment based on the joint use of a deep-towed seismic device (SYSIF) and seafloor instruments (OBH) to achieve seismic depth imaging in deep water. The experiment conducted during the ERIG3D cruise was directed at assessing the feasibility and demonstrating the added value of this original approach to the characterization of a buried Mass Transport Complex (MTC) offshore Nigeria.

This original configuration of the experiment combined with advanced processing succeeds in reaching lateral and vertical resolution (2.5 and 1 m respectively) in accordance with the objective of correlation with *in situ* measurement. The improvement of the vertical resolution was obtained by the use of signature deconvolution that exploits the full potential of the source of the deep-towed seismic system (i.e Janus-Helmholtz transducer). The improvement in lateral resolution was achieved via a depth imaging approach that enables the physical limitation of the Fresnel zone that affects singlefold sections to be overcome. Depth imaging requires the determination of the P-wave velocity distribution; this was achieved through the adaptation of an iterative focusing approach to the particular acquisition geometry. The success of the depth imaging approach lies mainly in an accurate determination of source and receiver positioning that is challenging in deep water. To reach the required accuracy, we used a relocation procedure based on the inversion of direct travel-times precisely determined by correlation with the measured source signature.

To illustrate the technological and processing advances of the proposed approach, we present a first application to the seismic data acquired over NG1, a buried Mass Transport Complex interpreted as a debris flow with 3D data and sub-bottom profiler data. Evidence for a slide nature of a part of the MTC may be advanced by the high resolution of the OBH depth images and the integration of the *in situ* measurements with the seismic data:

- Rigid behaviour may be inferred from movement of coherent material inside the MTC and thrust structures at the base of the MTC.
- A disrupted silt layer that maintains its stratigraphic position may support short transport dis-

tances. This silt layer is identified through the correlation of high resolution OBH images and geotechnical measurements, and confirmed by the matching of a deep-towed profile and a density log.

From the joint SYSIF/OBH experiment, several technical and methodological insights may also be highlighted. The feasibility to perform high resolution depth imaging of deep-towed data with fixed receivers and accurate positioning has been demonstrated. The main limitations of this approach are the duration of the experiment (deployment of seafloor instruments and definition of the deep-towed device track) and the short (200 m) profile investigated. To overcome these limitations, an upgrade of the SYSIF is necessary to include multichannel capabilities. The main challenge is to provide engineering data able to accurately monitor the shape of the streamer and hence the receiver positions. As revealed by this MTC case study, the geophysical characterization achieved by multi-offset deep-towed acquisition will, in the near future, be an essential tool in the evaluation and understanding of Geohazards in deep water for academic and industrial purposes.

## ACKNOWLEDGMENTS

This work benefited from the invaluable support of TOTAL colleagues *Didier Drapeau and Sylvie Delisle*. The SYSIF development and field experiments were conducted with the help of *Laurent Artzner, Yves Le Gall, Pierre Leon, Henri Martinossi, Eric Menut, Jean-Pierre Regnault* and *Yannick Thomas* from IFREMER. The OBH deployment was achieved with the help of Jacques Crozon, Mickael Roudaut and Pascal Pelleau from IFREMER. IFREMER and TOTAL financially supported this work through the ERIG3D project. The authors wish to thank *N. Wardell* for his help in improving the manuscript.

## REFERENCES

- Al-Yahya, K., 1989. Velocity Analysis by Iterative Profile Migration. *Geophysics*, **54**, 718-729.
- Auffret, Y., Pelleau, P., Klingelhoefer F., Geli, L., Crozon, J., Lin J.Y., Sibuet, J.-C., 2004. MicroOBS, a new generation of ocean bottom seismometer, *First Break*, **22**, issue 7.
- Bowen, A. N., 1984. A High Resolution seismic profiling system using a deep towed horizontal hydrophone streamer, *Mar. Geophys. Res.*, **6**, 275-293.
- Bull, S., Cartwright, J.A., Huuse M., 2009. A review of kinematic indicators from mass-transport complexes using 3D seismic data, *Marine and Petroleum Geology*, **26**, issue 7, 1132-1151.
- Briggs, S. E., Davies, R. J., Cartwright, J. A., Morgan, R., 2006. Multiple detachment levels and their control on fold styles in the compressional domain of the deepwater west Niger Delta, *Basin Research* **18**, 435-450.
- Brittle, K.F., Lines, L.R. and Dey, A.K., 2001. Vibroseis deconvolution: a comparison of cross-correlation and frequency-domain sweep deconvolution. *Geophysical Prospecting*, **49**, Issue 6, 675-686.

- Byrd, R.H., Schnabel, R.B., Shultz, G.A., 1988. Approximate Solution of the Trust Region Problem by Minimization over Two-Dimensional Subspaces, *Mathematical Programming*, **40**, 247-263.
- Calvès, G., Huuse, M., Schwab, A., Clift, P., 2008. Three-dimensional seismic analysis of high-amplitude anomalies in the shallow subsurface of the Northern Indus Fan: Sedimentary and/or fluid origin. *Journal of Geophysical research*, **113**, B11103.
- Canals, M., Lastras, G., Urgeles, R., Casamor, J.L., Mienert, J., Cattaneo, A., De Batist, M., Hafliadason, H., Imbo, Y., Laberg, J.S., Locat, J., Long, D., Longva, O., Masson, D.G., Sultan, N., Trincardi, F., Bryn, P., 2004. Slope failure dynamics and impacts from seafloor and shallow sub-seafloor geophysical data: case studies from the COSTA project. *Marine Geology-COSTA 213* (1-4), 9-72.
- Cartwright, J.A., 2007. The impact of 3D seismic data on the understanding of compaction, fluid flow and diagenesis in sedimentary basins. *Journal of the Geological Society*, London, **164**, 2007, 881-893
- Chapman, N.R., Gettrust, J.F., Walia, R., Hannay, D., Spence, G. D., Wood, W. T., Hyndman, R. D., 2002. High Resolution deep-towed multichannel seismic survey of deep sea gas hydrates off western Canada, *Geophysics*, **67**, 1038-1047.
- Claerbout, J. F., 1985, *Imaging the Earth's Interior*, Blackwell Scientific Publications, New York.
- Corredor, F., Shaw, J., Bilotti, F., 2005. Structural styles in the deep-water fold and thrust belts of the Niger Delta. *AAPG Bulletin* 89, 753-780.
- Davies, R.J., Clark, I. R., 2006. Submarine slope failure primed and triggered by silica and its diagenesis. *Basin Research*, **18**, 339-350.
- Dillon, P.B. and Thomson, R.C., 1984. Offset source VSP surveys and their image construction: *Geophysical Prospecting*, **32**, 790-811.
- Evamy, B.D., Haremboure, J., Kamerling, P., Knaap, W.A., Molloy, F.A. and Rowlands, P.H., 1978. Hydrocarbon habitat of Tertiary Niger Delta. *AAPG Bulletin*, 62, 1-39.
- Fagot, M. G., 1983. A deep-towed sound source and hydrophone array system: performance, prediction analysis and hardware description, in Pace M. (ed.), *Acoustics and the Seabed*, Bath Univ. Press, New York, 369-377.
- Garziglia, S., Sultan, S., Cattaneo, A., Ker, S., Marsset, B., Riboulot, V., Voisset, M., Adamy, J., Unterseh S. 2009. Identification of shear zones and their causal mechanism using a combination of cone penetration tests and seismic data in the Eastern Niger Delta. In : Mosher D., Locat J., Urgeles R. (eds) *Submarine Mass Movements and Their Consequences*. Springer Science. *Advances in Natural and Technological Hazards Research*, **28**, p 45-55.
- Gettrust, J. F., Ross, J. H., Rowe, M. M., 1991. Development of a low frequency deep-tow geoacoustics system, *Sea Technology*, 32, 23-32.
- Gettrust, J. F., Wood, W., Spsychalski, S., 2004. High-resolution MCS in deepwater: *The leading Edge*, **23**, 374-377.
- Haack, R.C., Sundararaman, P., Diedjomahor, J.O., Xiao, H., Gant, N.J., May, E.D. and Kelsch, K., 2000. Niger Delta petroleum systems, Nigeria. In: Mello, M.R. and Katz, B.J. (eds) *Petroleum systems of South Atlantic margins*. *AAPG*, 73, 213-232.

- He, T., Spence G., Wood, W., Riedel, M., Hyndman R., 2002. Imaging a hydrate-related cold vent offshore Vancouver Island from deep-towed multichannel seismic data, *Geophysics*, **74**, B23-B26.
- Heggland, R., 2004. Definition of geohazards in exploration 3-D seismic data using attributes and neural-network analysis. AAPG Bull., **88**, 857-868.
- Hooper, R.J., Fitzsimmons, R.J., Grant, N., and Vendeville, B., 2002. The role of deformation in controlling depositional patterns in the south-central Niger Delta, West Africa: *Journal of Structural Geology*, **24**, p. 847-859.
- Ker, S., Le Gall, Y., Marsset, T., and Leon, P., 2008. SYSIF, a low frequency seismic profiler for near-bottom marine geophysics, 70th EAGE Conference and Exhibition, Rome.
- Knox, G.J., and Omatsola, E.M., 1989. Development of the Cenozoic Niger Delta in terms of the 'Escalator Regression' model and impact on hydrocarbon distribution. Proceedings of the KNGMG Symposium 'Coastal Lowlands, Geology and Geotechnology'. Kluwer Academic Publishers, Dordrecht, 181-202.
- Kvalstad, T.J. 2007. What is the Current "Best Practice" in Offshore Geohazard Investigations? A State-of-the-Art Review In: Conference, O.T. (Ed.), Offshore Technology Conference. OTC, Houston, Texas, p. 18545.
- Le Gall, Y., 1999. Low-frequency Janus-Helmholtz transducer for great-depth acoustical oceanography. Proceedings of Sonar Transducers'99, Institute of Acoustics.
- Marsset, T., Marsset, B., Ker, S., Thomas, Y., Le Gall, Y., 2010. High and very high resolution deep-towed seismic system: Performance and examples from deepwater Geohazard studies. Deep-Sea Research I, doi:10.1016/j.dsr.2010.01.001.
- McClay, K., Dooley, T. and Zamora, G., 2003. Analogue models of delta systems above ductile substrates. In: van Rensbergen, P., Hillis, R.R., Maltman, A.J. and Morley, C.K. (eds) Subsurface Sediment Mobilization. Geological Society, London, Special Publications, **216**, 411-428.
- Molyneux, J. and Schmitt D., 1999. First-break timing: Arrival onset times by direct correlation, *Geophysics*, **64**, NO. 5, 14921501.
- Morley, C.K., 2003. Mobile shale related deformation in large deltas developed on passive and active margins. In: van Rensbergen, P., Hillis, R.R., Maltman, A.J. and Morley, C.K. (eds) Subsurface Sediment Mobilization. Geological Society, London, Special Publications, 216, 335-357.
- Nouzé, H, Sibuet, J-C, Savoye, B., Marsset B., and Thomas, Y., 1997. Pasisar: Performances of a High and Very High Resolution Hybrid Deep-Towed Seismic Device, *Marine Geophysical Researches*, **19**, Number 5, 379-395.
- Podvin, P. and Lecomte, I., 1991. Finite difference computation of travel times in very contrasted velocity models: A massively parallel approach and its associated tools, *Geophys, J, Int.*, **105**, 271-284.
- Quinn, R., Bull, J.M. and Dix, J.K., 1998. Optimal Processing of Marine High-Resolution Seismic Reflection (Chirp) Data. *Marine Geophysical Researches*, **20**, 13-20.
- Ramsey, N., 2002. A calibrated model for the interpretation of cone penetration tests (CPTs) in North Sea Quaternary soils. In: 'Offshore site investigation and geotechnics: diversity and sustainability', London.
- Rowe, M. M., and Gettrust, J.F., 1993. Fine structure of methane hydrate-bearing sediments on the Blake outer

- ridge as determined from deep-towed multichannel seismic data: *J. Geophys. Res.*, **98**, 463-473.
- Scales, J., 1997, *Theory of seismic Imaging*, Samizdat Press.
- Schneider, W., A., 1978. Integral formulation of migration in two and three dimensions, *Geophysics*, **43**, 49-76.
- Steihaug, T., 1983. The Conjugate Gradient Method and Trust Regions in Large Scale Optimization, *SIAM Journal on Numerical Analysis*, **20**, 626-637.
- Sultan, N., Voisset, M., Marsset, T., Vernant, A. M., Cauquil, E., Colliat, J. L., and Curinier, V., (2007). Detection of free gas and gas hydrate based on 3D seismic data and cone penetration testing: An example from the Nigerian Continental Slope, *Marine Geology*, **240** (1-4), 235-255.
- Taylor, J. R., 1982. *An introduction to error analysis*: Univ. Science Books.
- Tripsanas, E.K., Piper, D.J.W., Jenner, K.A., Bryant, W.R., 2008. Submarine mass-transport facies: new perspectives on flow processes from cores on the eastern North Atlantic margin. *Sedimentology*, **55**, 97-136.
- Walia, R. and Hannay, D., 1999. Source and receiver geometry corrections for deep-towed multi-channel seismic data, *Geophys. Res. Lett.*, **26**, 1993-1999.
- Westbrook, G., Exley, R., Minshull, T., Nouzé, H., Gailler, A., Jose, T., Ker S., and Plaza A., 2008. High-Resolution 3D seismic investigations of hydrate-bearing fluid-escape chimneys in the Nyegga region of the Voring Plateau, Norway, Proceedings of the 6th International Conference on Gas Hydrates (ICGH 2008), Vancouver, July 6-10.
- Wood, W., and Gettrust J.F., 2001. Deep-tow seismic investigations of Methane Hydrates, Natural Gas Hydrate: Occurrence, Distribution, and Detection, Geophysical Monogram 124.
- Wood, W., Gettrust J.F., Sychalski, S., 2003, A new deep-towed, multi-channel seismic system. *Sea Technology*, **44**, 44-49.
- Wood, W., Hart, P., Hutchinson, D., Dutta., N., Snyder, F., Coffin, R., Gettrust, J., 2008. Gas and gas hydrate distribution around seafloor seeps in Mississippi Canyon, Northern Gulf of Mexico, using multi-resolution seismic imagery, *Marine and Petroleum Geology*, **25**, 952-959.
- Yilmaz, O., 1987, *Seismic Data Processing*, Society of Exploration Geophysicists, Tulsa Oklahoma.
- Yoerger, D., Jakuba, M., Bradley., A., Bingham, B., 2007. Techniques for Deep Sea Near Bottom Survey Using an Autonomous Underwater Vehicle, *Robotics Research*, 416-429.
- Ziolkowski, A., 1991. Why dont we measure seismic signatures?: *Geophysics*, **56**, 190-201.

## FIGURE CAPTIONS

Figure 1: a. Seabed dip map showing in grey the areal extension of the distal part of NG1. Location of the seismic data, cores and *in situ* measurements collected during the ERIG3D cruise. b. Close-up of the location map showing the data used in this study.

Figure 2: Picture of the SYSIF heavy towed vehicle during a JH250-6000 deployment.

Figure 3: OBH 3 before (left) and after (right) the correction of the jitter related to the source position variations.

Figure 4: a) Correlation coefficient for OBH data calculated with farfield signature b) Power spectral density of the direct waveform for OBH3.

Figure 5: a) Mean Source signature recorded in farfield condition. b) Power Spectral Density of the source signature.

Figure 6: Left: Correlation processing (filter 350-1100 Hz). Right: Deconvolution processing (filter 200-1100 Hz).

Figure 7: Semblance analysis performed on OBH 3. The OBH data were split in two sets (positive and negative offsets). A quasi constant velocity characterizes the first 200 ms below the seabed. After 200 ms, one can observe the difference in the velocity estimate.

Figure 8: Velocity scan performed on OBH3. OBH3 was migrated with close constant velocities (1460, 1470, 1480, 1490 and 1500 m/s). The change in shape of reflectors unveils sensitivity finer than 10 m/s. A velocity of 1480 m/s ensures the correct depth migration of the shallow part of the section (up to 840 m) which includes the MTC NG1.

Figure 9: Depth Migrated OBH3 section and interval velocities obtained by the iterative depth migration approach. Dotted lines are the uncertainties on the velocity values. *In situ* velocity measurements from Vp13S03 (Penfeld Penetrometer data) are displayed in bold black. This *in situ* measurement confirms the close to homogeneous behaviour of the velocity distribution in the upper part of the section.

Figure 10: Comparison between the streamer time section and a stack of OBH depth images

Figure 11: Comparison between the hull-mounted sub-bottom profiler CH18 and the VHR SYSIF profile SY13-Pr01. This comparison illustrates the increase in lateral resolution obtained by the deep-towed acquisition.

Figure 12: Top left: Seismic line extracted from a 3D cube. Bottom left: AUV sub-bottom profiler line [1800-5000 Hz]. Right: SYSIF line [220-1050 Hz].

Figure 13: Depth migrated OBH Receiver gathers. White arrows indicate the location of NG1 top characterized by a set of high amplitude reflection alternating with zones of lower reflectivity. Note the thrust structures at the base of NG1.

Figure 14: Integrated HR seismic, OBH depth image, core and log data. On the density log of the borehole BH-FP7 tied to the SY10-HR-Pr01 line and presented on the left side of the figure, the values vary in the range [1.16-1.62  $\text{g.cm}^{-3}$ ]. The projected location of the CPT09S05 is shown on both the SY10-HR-Pr01 line and the OBH3 depth image. The three logs of the CPT09S05 presented include the corrected cone resistance,  $q_t$ , the excess pore-water pressure induced by the penetration of the cone,  $\Delta u_2$ , and the interpretation of the sediment types derived from these measurements using the calibrated model of Ramsey (2002).



**Table 1.** Geophysical Tools used during the ERIG3D cruise and acquisition parameters

Seismic Device	Frequency / duration (Hz) / (ms)	Altitude (m)	Shooting Rate (s)	Ship Speed (Kn)	SL (dB $\mu$ Pa@1m)	Line Name
Sysif JH650-6000	[580-2200]/50	60	2.4	2	196	SY13-VHR-Pr01
Sysif JH250-6000	[220-1050]/100	150	2.6	1	196	SY10-HR-Pr01
Sysif/OBH	[220-1050]/100	150	2.6	1	196	SY10-HR-Pr01
Chirp (Hull)	[1800-5000]/50	Surface	1	5	210	CH18
Chirp (AUV)	[1800-5000]/50	80	1.3	3	190	AUV03-Pr16

**Table 2.** Residuals (mean values in ms) obtained after each step of the relocation procedure for the five OBHs

Step	OBH1	OBH2	OBH3	OBH4	OBH5
Initial	1.69	2.12	1.92	0.70	1.14
Step 1	0.32	0.34	0.36	0.65	0.93
Step 2	0.31	0.23	0.32	0.31	0.6

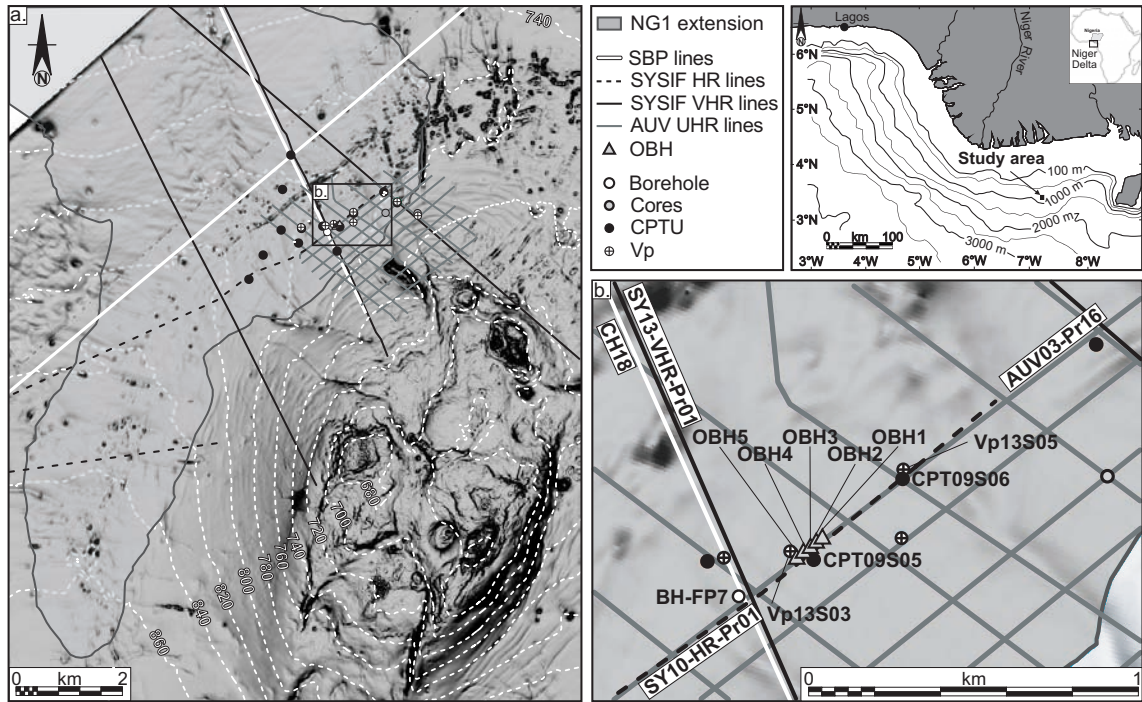


**Figure 1.** a. Seabed dip map showing in grey the areal extension of the distal part of NG1. Location of the seismic data, cores and *in situ* measurements collected during the ERIG3D cruise. b. Close-up of the location map showing the data used in this study.

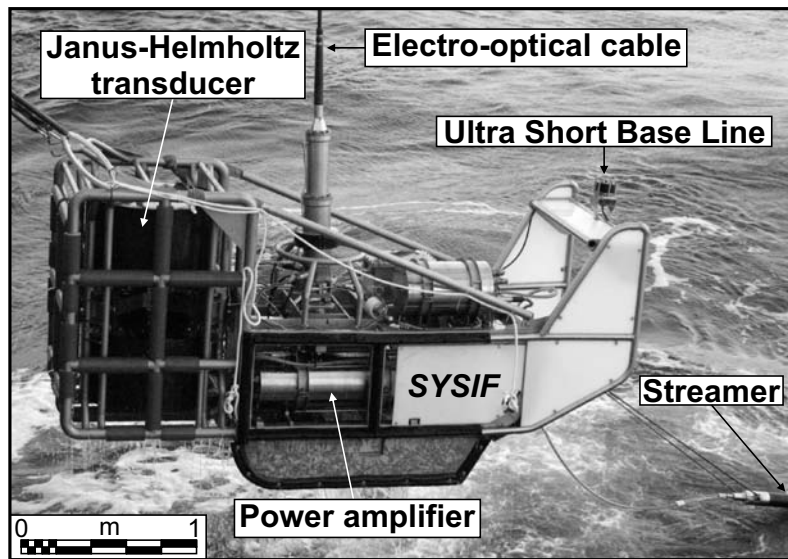


Figure 2. Picture of the SYSIF heavy towed vehicle during a JH250-6000 deployment.

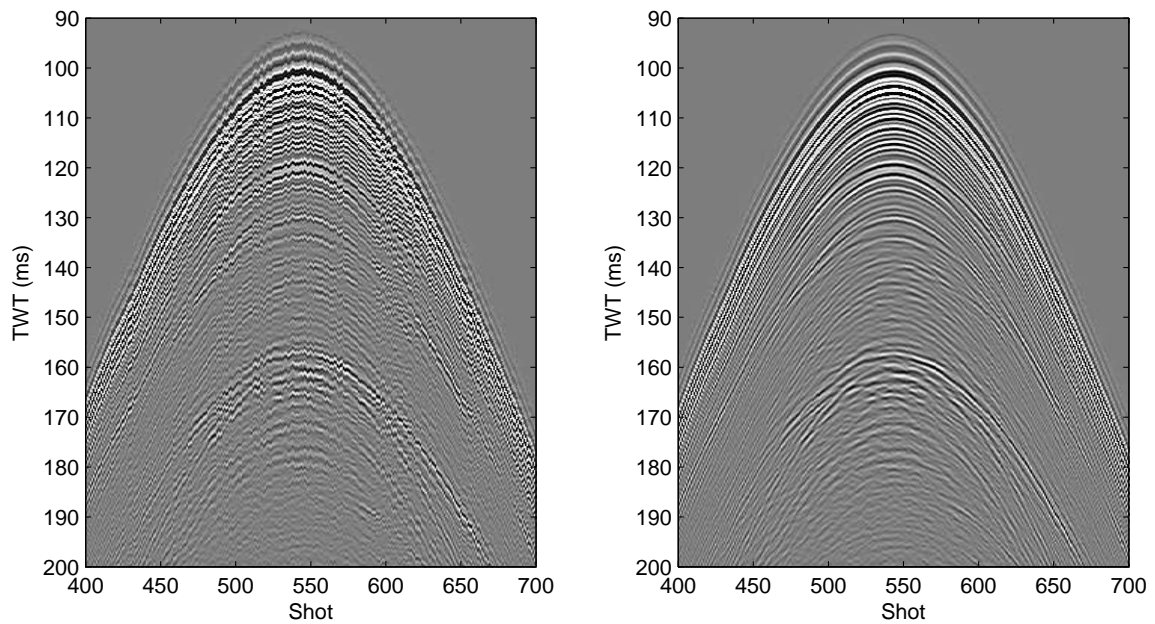
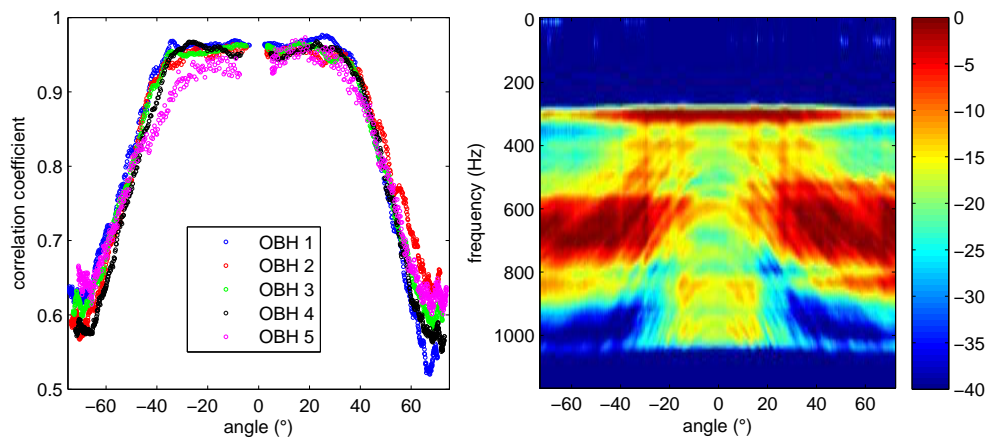
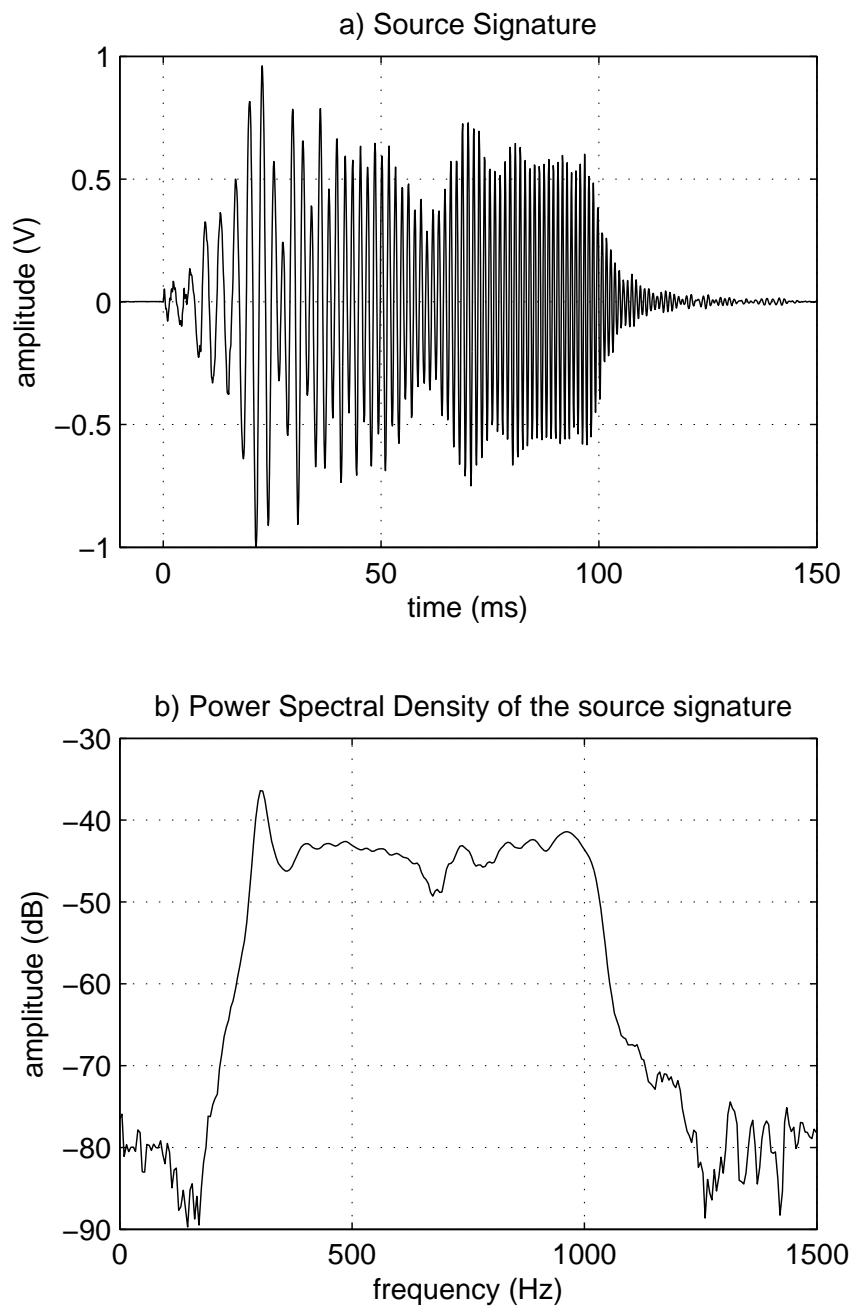


Figure 3. OBH 3 before (left) and after (right) the correction of the jitter related to the source position variations.



**Figure 4.** a) Correlation coefficient for OBH data calculated with farfield signature b) Power spectral density of the direct waveform for OBH3



**Figure 5.** a) Mean Source signature recorded in farfield condition. b) Power Spectral Density of the source signature.

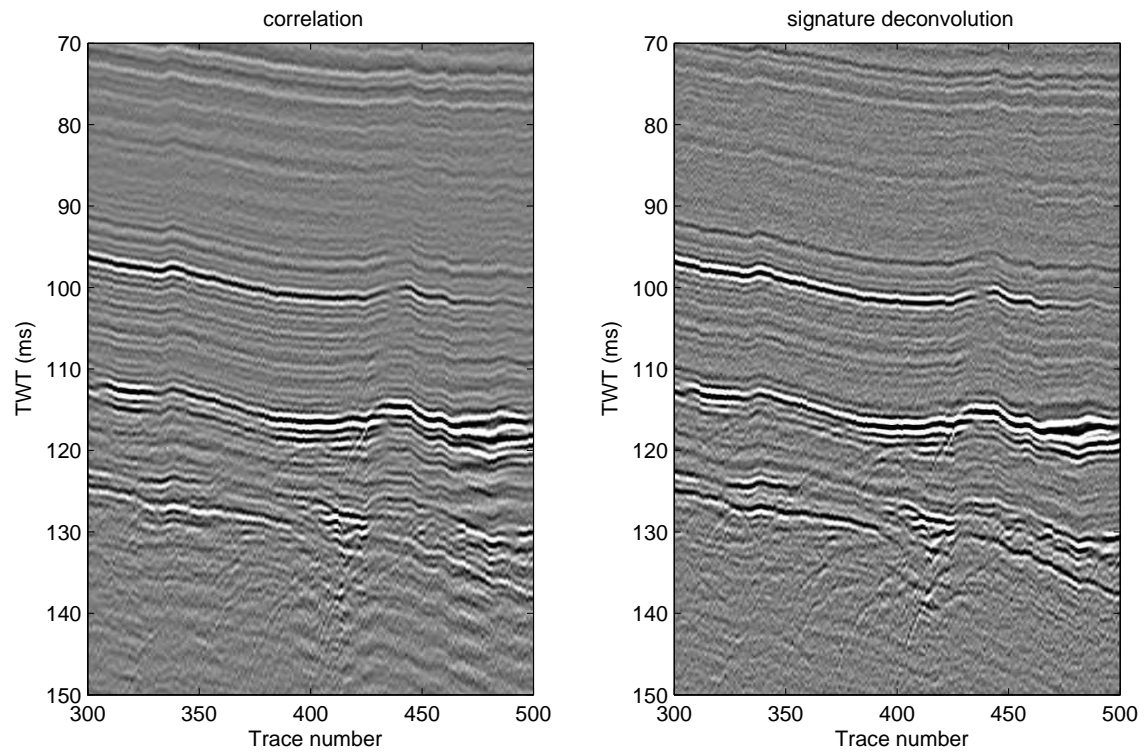


**Figure 6.** Left: Correlation processing (filter 350-1100 Hz). Right: Deconvolution processing (filter 200-1100 Hz).

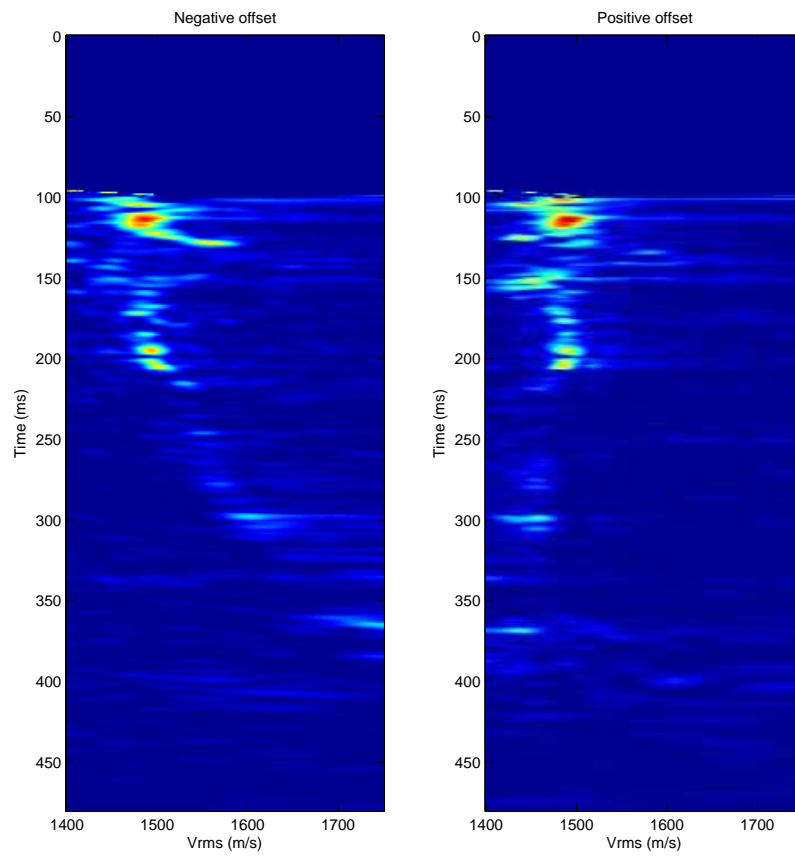


**Figure 7.** Semblance analysis performed on OBH 3. The OBH data were split in two sets (positive and negative offsets). A quasi constant velocity characterizes the first 200 ms below the seabed. After 200 ms, one can observe the difference in the velocity estimate.

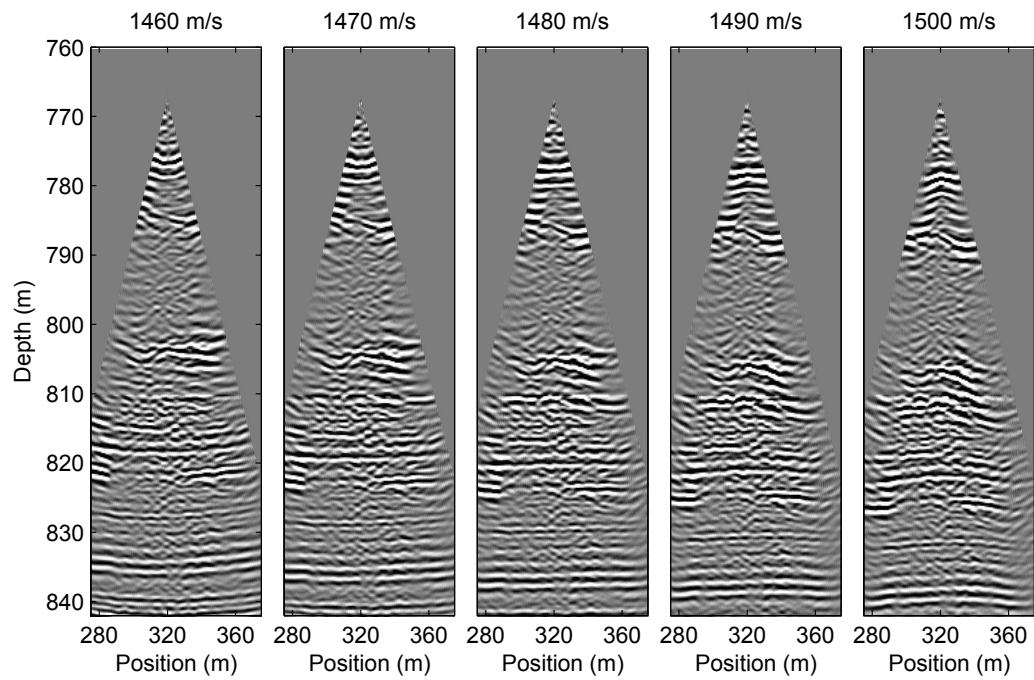


**Figure 8.** Velocity scan performed on OBH3. OBH3 was migrated with close constant velocities (1460, 1470, 1480, 1490 and 1500 ms). The change in shape of reflectors unveils sensitivity finer than 10 m/s. A velocity of 1480 m/s ensures the correct depth migration of the shallow part of the section (up to 840 m) which includes the MTC NG1.



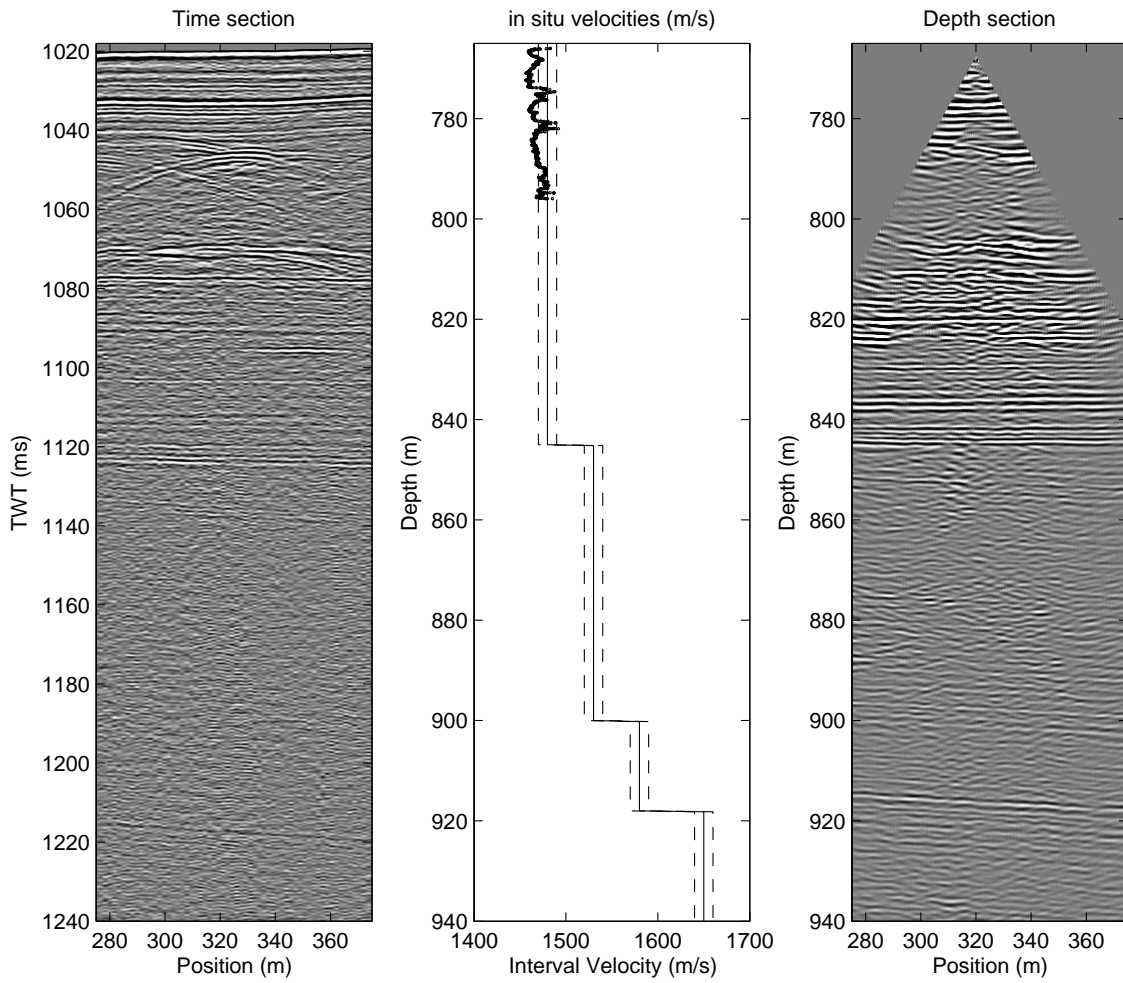


**Figure 9.** Depth Migrated OBH3 section and interval velocities obtained by the iterative depth migration approach. Dotted lines are the uncertainties on the velocity values. *In situ* velocity measurements from Vp13S03 (Penfeld Penetrometer data) are displayed in bold black. This *in situ* measurement confirms the close to homogeneous behaviour of the velocity distribution in the upper part of the section.

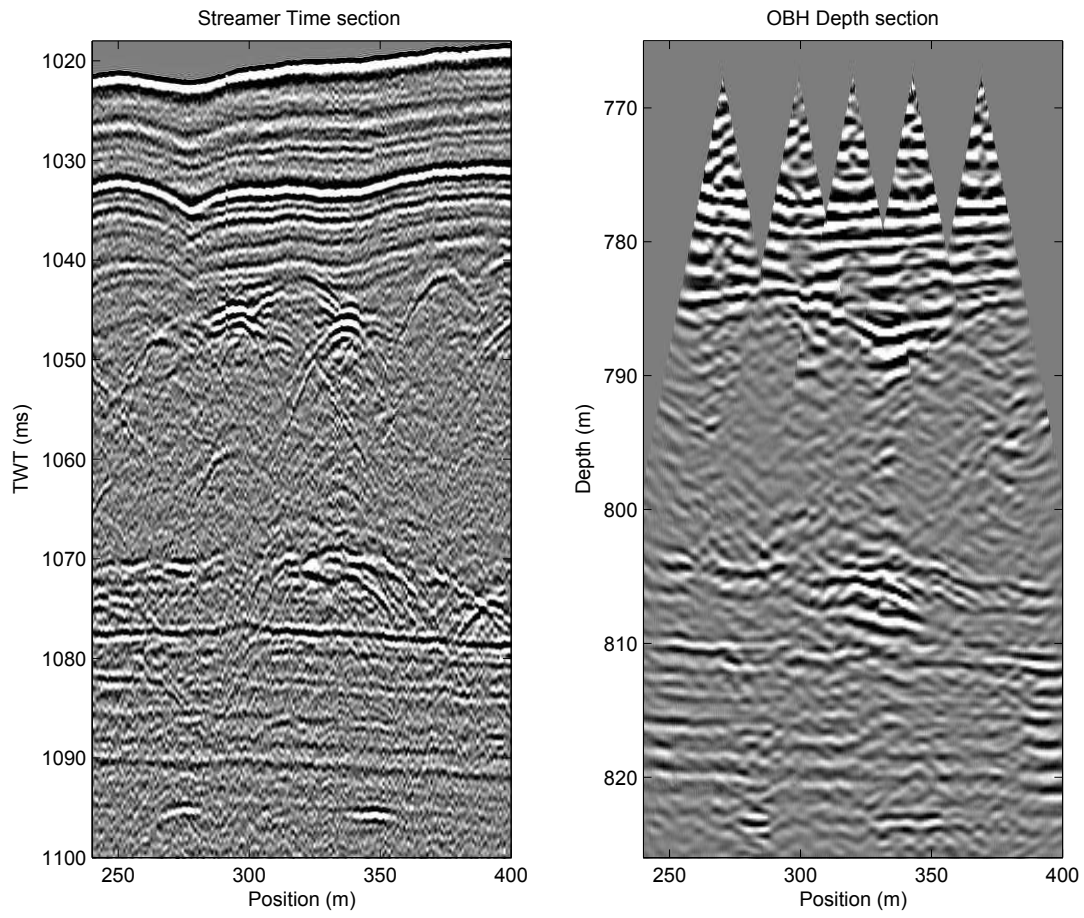


**Figure 10.** Comparison between the streamer time section and a stack of OBH depth images

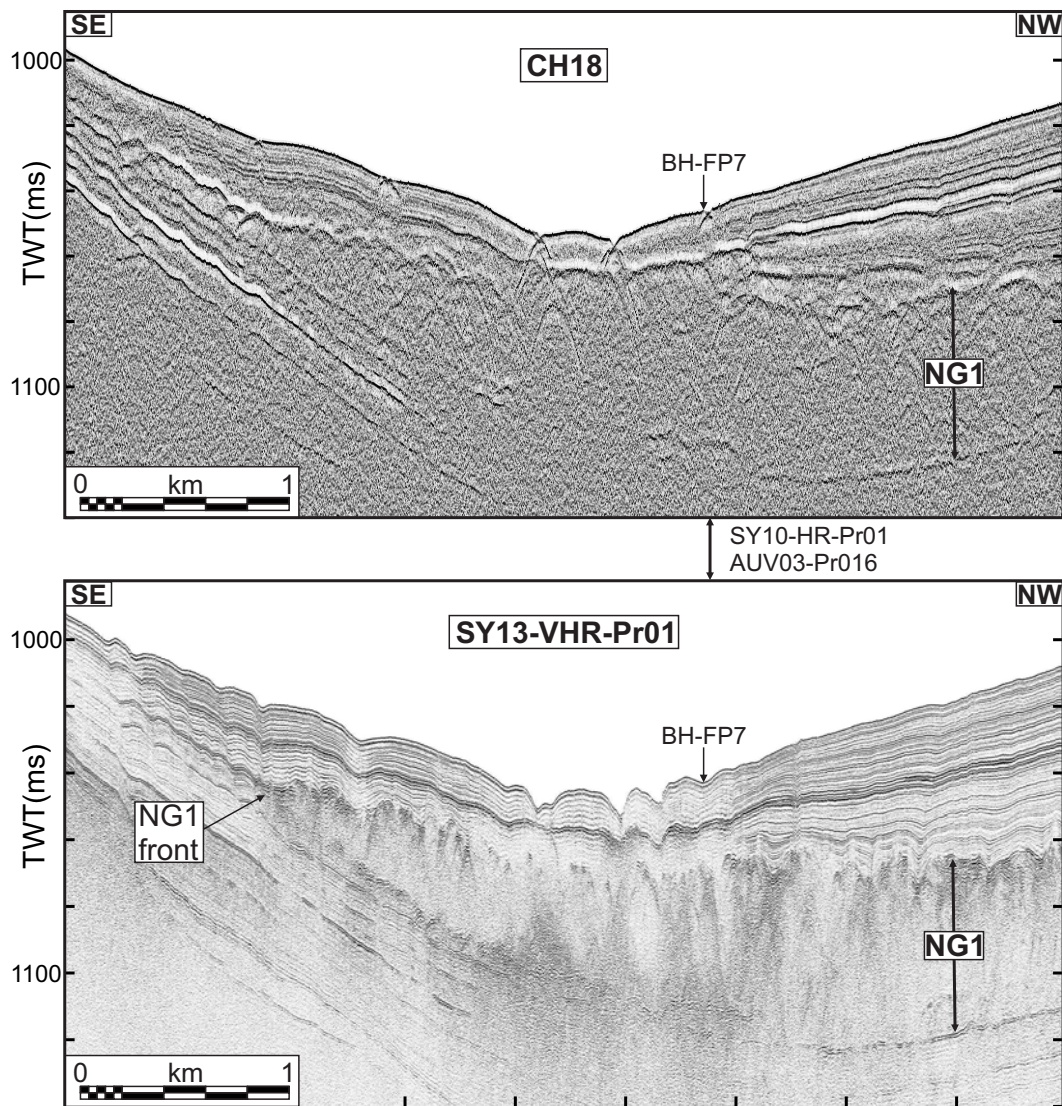


**Figure 11.** Comparison between the hull-mounted sub-bottom profiler CH18 and the VHR SYSIF profile SY13-Pr01. This comparison illustrates the increase in lateral resolution obtained by the deep-towed acquisition.

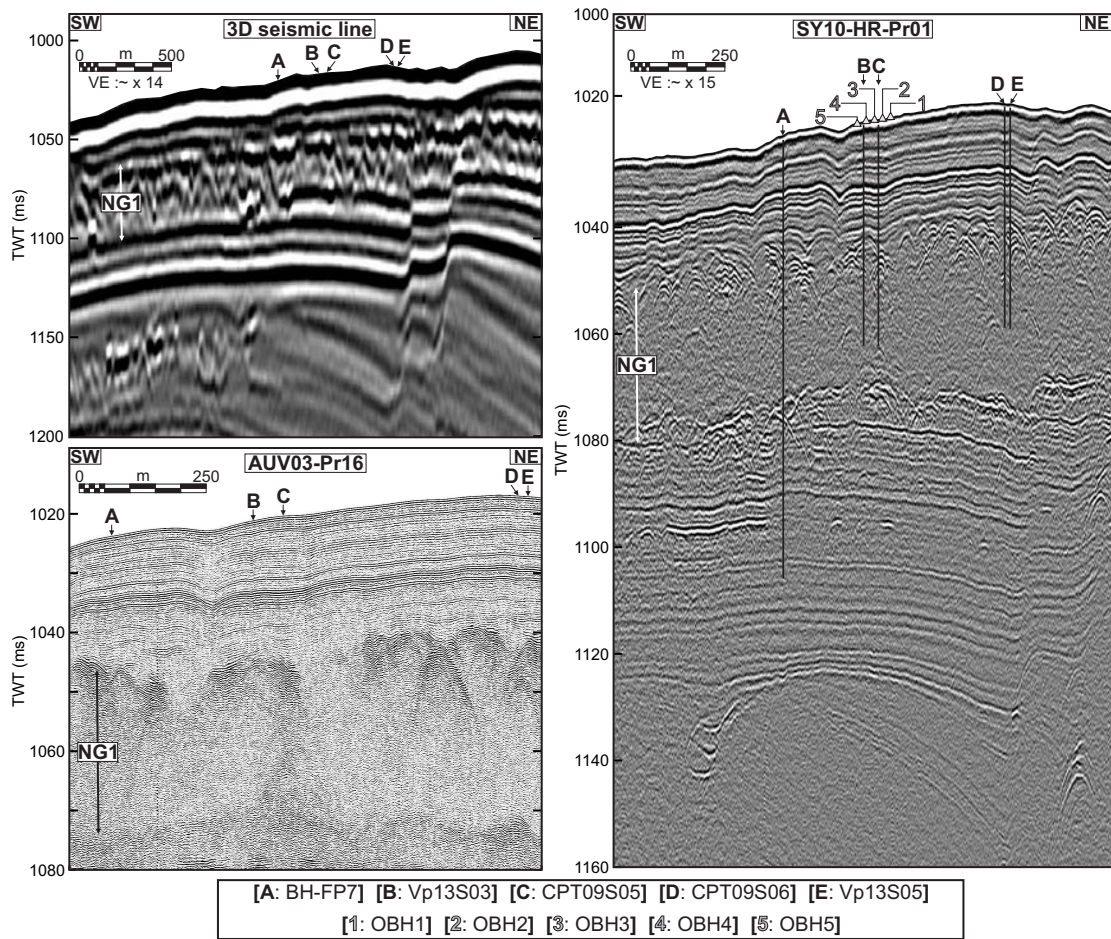


**Figure 12.** Top left: Seismic line extracted from a 3D cube. Bottom left: AUV sub-bottom profiler line [1800-5000 Hz]. Right: SYSIF line [220-1050 Hz].

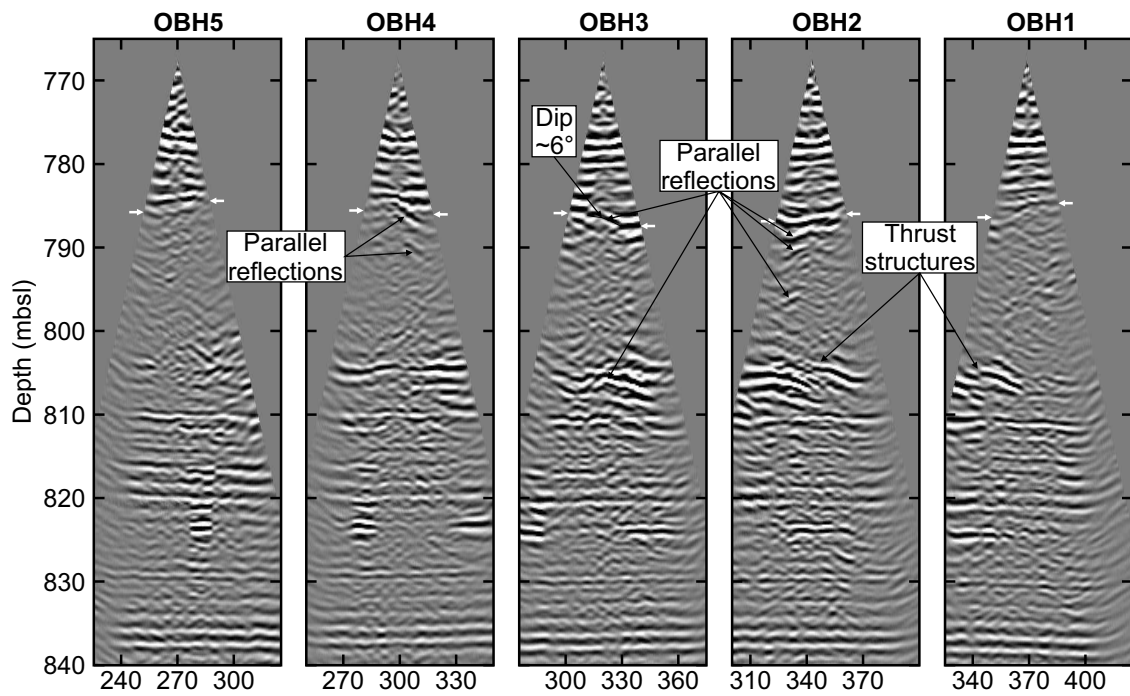


**Figure 13.** Depth migrated OBH Receiver gathers. White arrows indicate the location of NG1 top characterized by a set of high amplitude reflection alternating with zones of lower reflectivity. Note the thrust structures at the base of NG1.

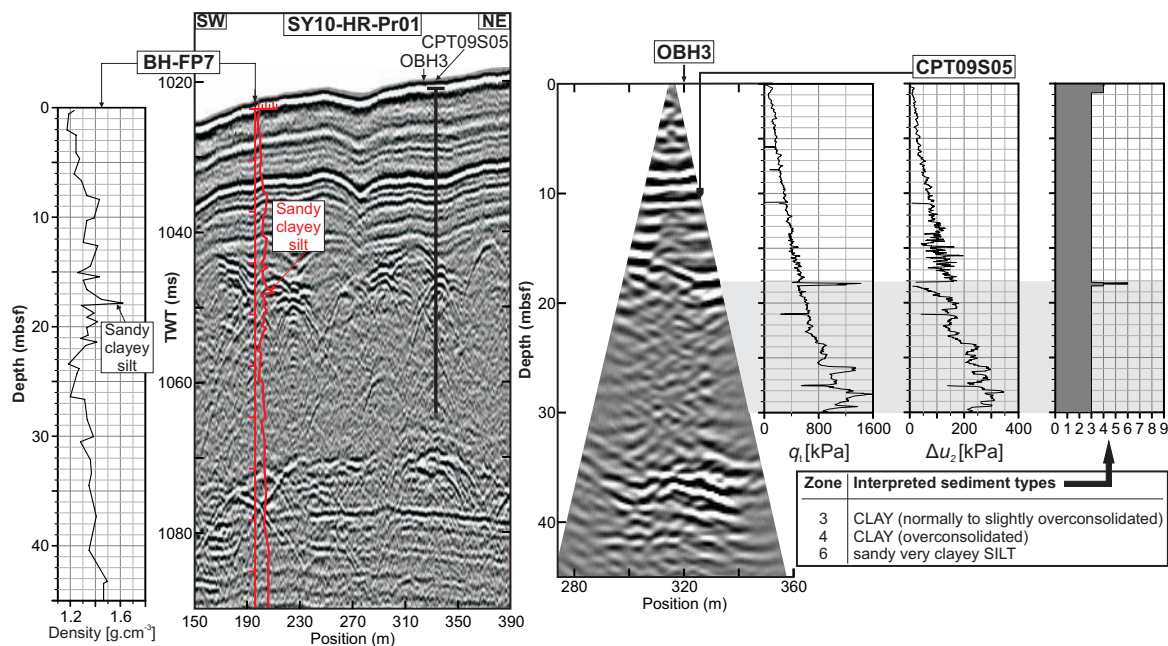


**Figure 14.** Integrated HR seismic, OBH depth image, core and log data. On the density log of the borehole BH-FP7 tied to the SY10-HR-Pr01 line and presented on the left side of the figure, the values vary in the range [1.16-1.62  $g.cm^{-3}$ ]. The projected location of the CPT09S05 is shown on both the SY10-HR-Pr01 line and the OBH3 depth image. The three logs of the CPT09S05 presented include the corrected cone resistance,  $q_t$ , the excess pore-water pressure induced by the penetration of the cone,  $\Delta u_2$ , and the interpretation of the sediment types derived from these measurements using the calibrated model of Ramsey (2002).